Fusion Engineering and Design 215 (2025) 114940

Contents lists available at ScienceDirect

Fusion Engineering and Design

journal homepage: www.elsevier.com/locate/fusengdes

Proposal of a criterion to select the layout of bolometric diagnostics for robust plasma radiation reconstruction in fusion devices

Ivan Wyss [a,*], Valentina D'Agostino [a], Andrea Murari [b,c], Pasquale Gaudio [a], Michela Gelfusa [a], Gerarda Apruzzese [d], Riccardo Rossi [a]

[a] *Università di Roma "Tor Vergata", Dipartimento di Ingegneria Industriale, Via del Politecnico 1, 00133 Rome, Italy*
[b] *Consorzio RFX (CNR, ENEA, INFN, Università di Padova, Acciaierie Venete SpA), Corso Stati Uniti 4, 35127 Padova, Italy*
[c] *Istituto per la Scienza e la Tecnologia dei Plasmi, CNR, Padova, Italy*
[d] *ENEA, Nuclear Department, Via Enrico Fermi 45, 00044 Frascati, Italy*

ARTICLE INFO

Keywords:
Bolometry
Plasma Radiation
Tomography
Plasma Diagnostic

ABSTRACT

Nuclear fusion stands out as a promising energy source, with numerous experimental reactors currently operational and larger ones in various stages of construction. As reactor dimensions increase, the precise measurement of the plasma total emitted radiation becomes increasingly crucial. This quantity not only helps in evaluating tokamak power balances but also enhances the understanding of the underlying physics in different processes. To optimize the performance of large nuclear fusion reactors, for example, various radiative scenarios have been proposed. These involve injecting gas into the plasma to induce radiation emission, thereby reducing the heat load on the reactor plasma facing components. Additionally, analysing the radiation pattern within the plasma provides valuable insights into impurity transport. A key technique for extracting information on plasma radiation is tomography reconstruction based on bolometric measurements. Addressing the resulting inverse problem, an effective approach involves utilizing maximum likelihood methods, which not only facilitates the reconstruction but also offers an estimation of the reconstruction errors. This study aims to investigate the impact of the bolometer diagnostic geometry on the reconstruction performance, a critical aspect for designing bolometers for future fusion machines. Due to limited space availability, bolometer systems present a restricted number of projections, rendering the optimization of the geometry fundamental for minimizing the sources of error. The analysis performed consists of reconstructing synthetic images in different geometries, varying angles of view and the number of lines of sight. Finally, an optimal criterion is defined to guide the selection of the geometry, ensuring robust reconstruction with minimal susceptibility to measurement errors.

1. Introduction

In tokamaks, radiation measurements provide fundamental information for plasma control and the study of its dynamics [1]. From these measurements, it is possible to identify the onset of instabilities that can lead to anomalous phenomena in the plasma [2–5]. Furthermore, understanding the plasma emission is essential for determining plasma energy losses and assessing the heat load on the divertor [6–8].

Diagnostic tools, such as bolometers or soft X-ray detectors, produce line-integrated measurements from different channels [9]. To extract meaningful spatial information, a tomographic inversion is required. In the field of tomography for fusion reactors, various approaches have been employed, such as Maximum Entropy [10], Minimum Fisher Information [11], and Gaussian Processes [12]. The quality of the reconstruction depends significantly on the geometry of the lines of sight observing the cross-section of the tokamak [13]. The design of the lines of sight is typically determined by reconstructing specific phantoms while considering the engineering constraints of plasma accesses [14–15]. Generally, the goal is to maximize the achievable resolution in the areas of interest by ensuring that multiple lines intersect these regions. This article demonstrates how the maximum likelihood tomography enables a more robust design of the diagnostic layout. Indeed, the maximum likelihood algorithm not only permits to estimate the emissivity but also accounts for the propagation of the uncertainties without relying on Monte Carlo methods, which are computationally intensive (Section 2). This can be used to assess the sensitivity of a given geometry

* Corresponding author.
E-mail address: ivan.wyss@uniroma2.it (I. Wyss).

https://doi.org/10.1016/j.fusengdes.2025.114940
Received 27 December 2024; Received in revised form 4 March 2025; Accepted 5 March 2025
Available online 18 March 2025

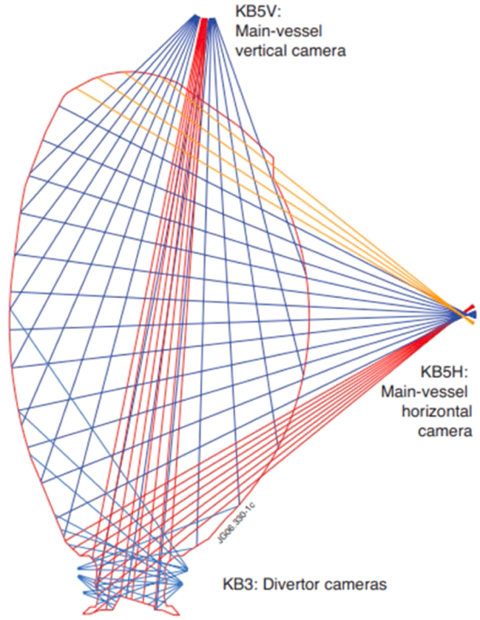

Fig. 1. Layout of JET Bolometer Diagnostic.

to the measurement errors [16]. Consequently, the maximum likelihood allows, during the design phase, an assessment of a given line-of-sight configuration, not only in terms of reconstruction accuracy but also regarding the sensitivity of the geometry to the measurement errors affecting the line integrals (Section 3). The objectives of the present work are to document this aspect for a JET like geometry and to introduce two indicators, the *geometric coverage* and the *error factor*, to quantify the quality of a given diagnostic layout (Section 4). These metrics can help finding the best trade-off between accuracy of the reconstructions and their vulnerability to measurement errors (Section 4). The proposed criteria are fully general, can be applied to other tomographic problems and can be extended to take into account also the uncertainties in the magnetic topology (Section 5).

2. Maximum likelihood tomography

In a tokamak, various diagnostics observe the plasma and provide integrated measurements. The geometry of the bolometric system on JET [17] is shown as an example in Fig. 1. The lines of sight are defined by the geometry of the detector and the collimator, and the resulting measurements are determined by the contribution of the radiation emitted along their entire line of sight. In reality, the radiation observed by the detectors does not originate from a single line but from an emission volume [18]. For this reason, it may be necessary to determine how each volume element contributes to the measurements, a task that can be performed using ray-tracing simulations [19]. In particular, the examples presented in this work will refer to the poloidal cross-section of JET. The goal of tomographic inversion is therefore to determine the emissivity field responsible for producing the measurements.

After discretizing the domain in pixels, the tomographic problem can be summarized with Eq. (1)

$$g = Hf \tag{1}$$

Here, g [W/m^2] represents the set of measurements, f [W/m^3] is the emissivity that we aim to reconstruct, and H is the geometry projection matrix, which defines the contribution of each pixel to each measurement. A brief explanation of the maximum likelihood principle is provided below; for further details, the interested reader is referred to [20–22].

The maximum likelihood tomography is one of the most widely used methods to perform tomographic reconstructions. The core idea is to maximize the likelihood L of obtaining the emissivity g given the set of m measurements g_m, as illustrated in Eq. (2).

$$L(g|f) = \prod_m L(g_m|f) \tag{2}$$

From Eq. (2) and assuming that the measurements g are affected by the noise n, whose uncertainty propagates into emissivity estimation, one can write:

$$g = \bar{g} + n \tag{3}$$

$$f = \bar{f} + \varepsilon \tag{4}$$

It is possible to demonstrate that an iterative estimation of the emissivity f and the associated uncertainty ε is provided by the following relations (5) and (6):

$$f^{k+1} = \frac{f^k}{H'1} \cdot H' \frac{g}{Hf^k} \tag{5}$$

$$\varepsilon^{\,k+1} = \left[I - A^k\right]\varepsilon^k + B^k n \tag{6}$$

In equations (5), the dot represents the element-wise product, while in the absence of a dot, the operation is understood as the standard matrix-vector product.Division is always intended as an element-wise operation. In an element-wise operation, each element of a vector is

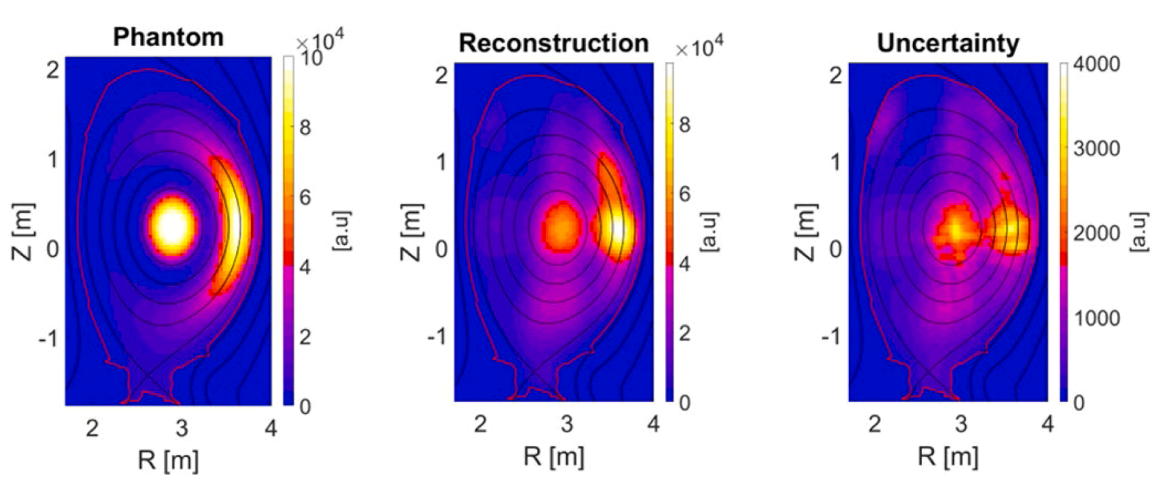

Fig. 2. Phantom (Left), Reconstruction (middle) and uncertainty (right) obtained with isotropic smoothing. The magnetic field lines are reported to guide the eye but are not used in the reconstruction.

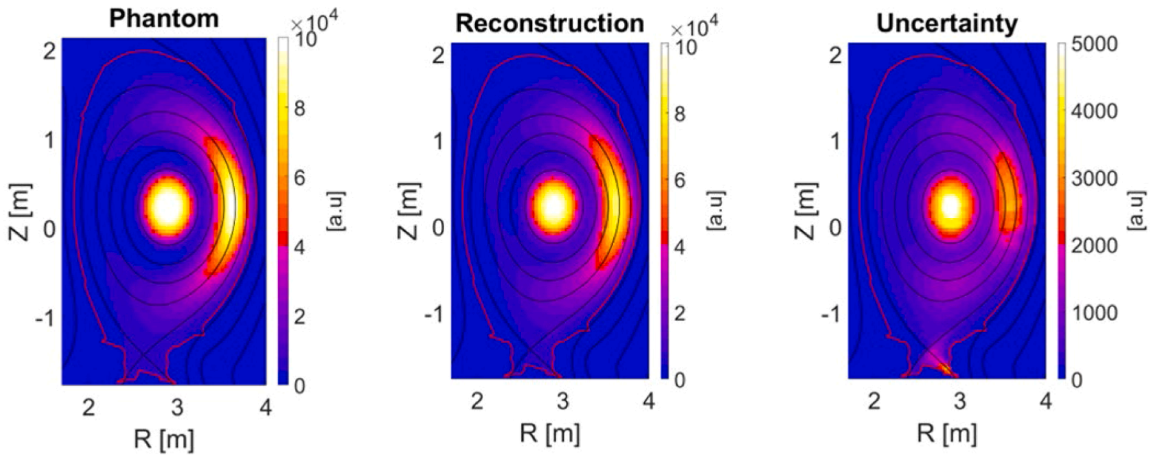

Fig. 3. Phantom (Left), Reconstruction(middle) and uncertainty(right) obtained by regularizing along the magnetic field lines.

multiplied or divided by the corresponding element of the other vector, resulting in a vector of the same dimension as the original two vectors. Meanwhile, **1** is a vector of ones of the same length as the number of projections, H′ is the transpose of the geometry projection matrix H and I is the identity matrix. The entries of the matrixes A and B are given by Eqs. (7) and (8).

$$A^k = \frac{f^k}{H'1Hf^k}H';H \tag{7}$$

$$B^k = \frac{f^k}{H'1Hf^k}H' \tag{8}$$

In tokamaks, the number of lines of sight is typically limited by the access constraints to the vacuum vessel. This means that the available information is underdetermined, making tomographic inversion a highly ill-posed problem [23]. To address this, it is necessary to introduce prior information to constrain the solutions. Various approaches exist in the literature [24]. One common method involves imposing smoothness on the radiation field, ensuring that the second derivatives along the x and y directions are zero. To evaluate the effectiveness of a method or geometry, given the ill-posed nature of the problem, synthetic cases called phantoms can be constructed. These allow deriving the expected measurements and then performing the inversion on this data. This approach provides a reference solution to compare against the results obtained. In the present work, since the phantoms are synthetic cases, all the indicators and uncertainties are expressed in arbitrary units.

Fig. 2 shows an example of an inversion obtained from the phantom on the left, along with the uncertainty propagation, using the introduced isotropic regularization but without any information about the magnetic topology.

An effective indicator for assessing the quality of the reconstruction

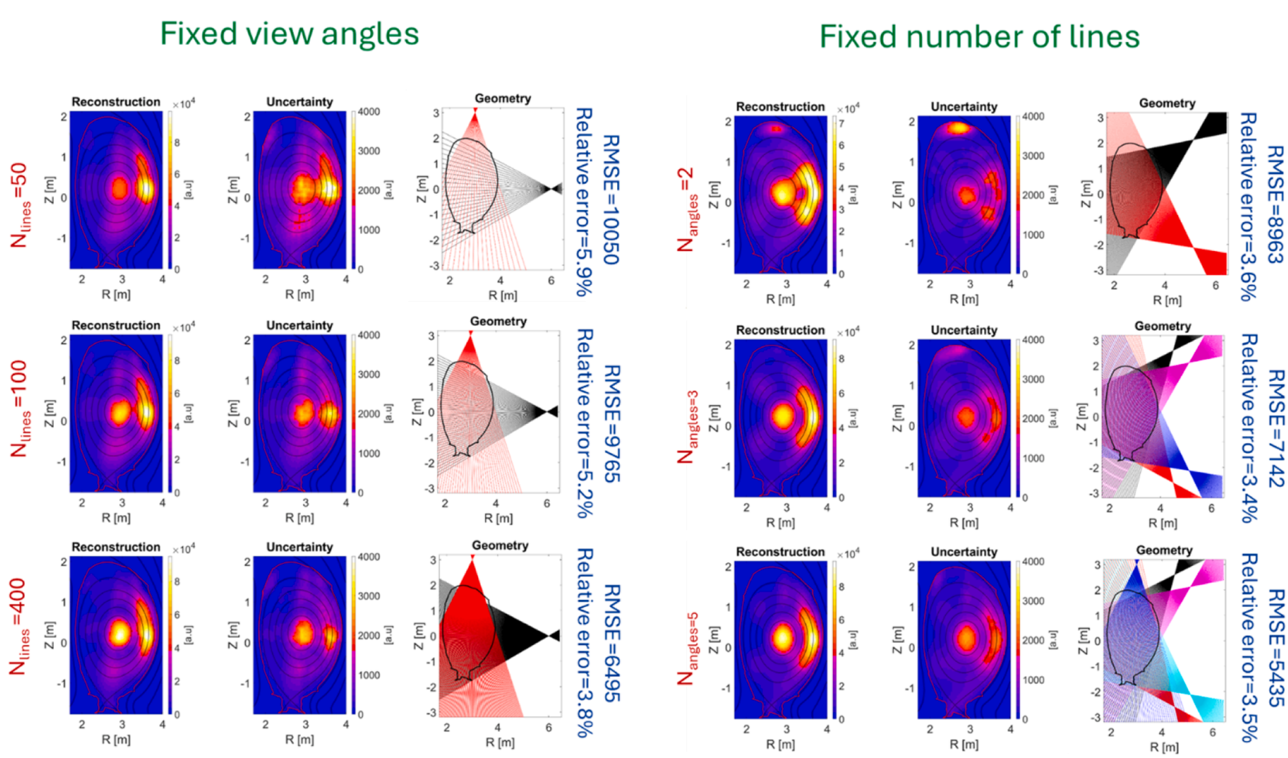

Fig. 4. (Left) Geometry with two fixed angles of view incrementing the number of lines of sight. (Right) Geometry with a fixed number of lines of sight increasing the number of viewing angles For each case the columns report: Reconstruction (Left), Uncertainty (Middle) and Geometry (Right).

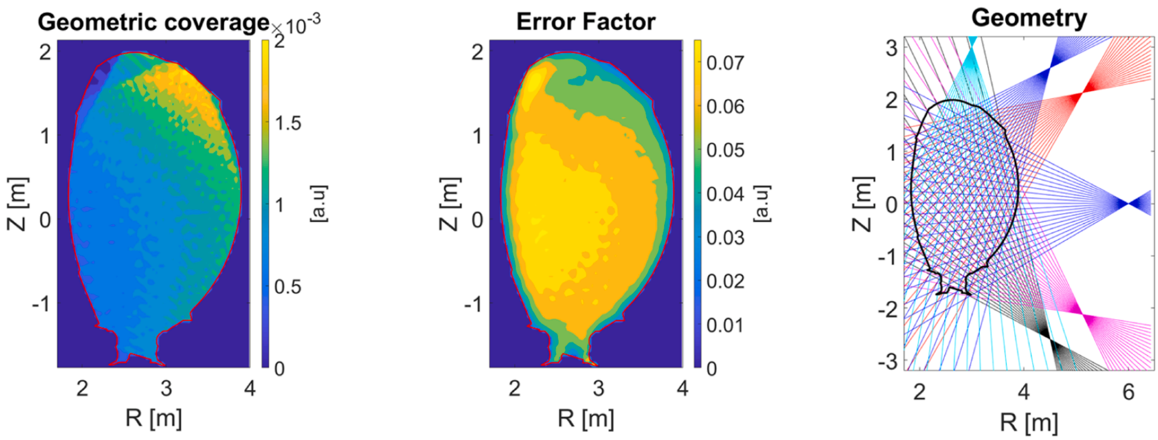

Fig. 5. Geometric coverage (Left) and Error factor (Middle) of the optimized geometry (Right).

is the Root Mean Square Error (RMSE) in (9). This metric indicates how close the reconstructed image is to the original one.

$$RMSE = \sqrt{\frac{1}{n_{pixels}} \sum_{i=1}^{n_{pixels}} \left(f_{phantom_i} - f_{reconstruction_i}\right)^2} \tag{9}$$

An additional indicator is introduced to estimate the impact of uncertainties: the relative uncertainty, defined as the ratio of the uncertainty ε divided by reconstructed emissivity $f_{reconstruction_i}$.

$$Relative\ uncertainty = \left(\frac{\varepsilon_i}{f_{reconstruction_i}}\right) \tag{10}$$

This value is evaluated for the pixels where the radiation exceeds a certain threshold to avoid overestimation. The average relative uncertainty is then the mean of the relative uncertainty mediated over the pixels with the emissivity above the threshold. In the present work the threshold has been chosen at the level of 20 % of the maximum emissivity. For the example of Fig. 2, the RMSE obtained is equal to 9765 [a.u.] and the average relative uncertainty is 5.2 %.

Another widely used approach involves imposing smoothness of the radiation along the magnetic field lines. In Fig. 3 the reconstruction and uncertainty obtained with this regularization is reported. The RMSE is obviously lower than previously because the phantom itself is smoothed along the magnetic field, but this is what is expected in the experiments. Furthermore, it is important to notice that the propagation of the uncertainties depends also on the regularisation.

For this example, the RMSE obtained is equal to 2427 [a.u] and the average relative uncertainty is 8.6 %.

Although the radiation is expected to be smoother along the magnetic field lines, introducing the magnetic topology as a prior constraint would not only increases computational demands but would also introduce a potentially confusing element (the results would depend on the configuration of the fields and the associated uncertainties). Consequently, to keep the treatment as simple and intuitive as possible, the isotropic regularization without any information about the magnetic field lines will be discussed in the following. This approach permits to converge on a sufficiently robust geometry that does not rely on the introduction of prior information.

3. Geometry design application

To show how incorporating the uncertainty propagation can improve the quality of the selected geometry, two representative examples are discussed in this section. In the first example, only two access points are available for viewing the cross-section, and the number of their lines of sight is varied. In the second example, the number of lines is fixed at 200, while the viewing angles are incrementally increased. The results are summarized in Fig. 4 for the case of the phantom reported in Fig. 3.

For each geometry, the obtained reconstruction is presented along with the uncertainty propagation, considering a 5 % relative measurement error. Additionally, the error of the reconstructed emissivity with respect to the phantom is reported, expressed in terms of RMSE and the average relative uncertainty. As expected, for the fixed viewing angles in Fig. 4 (left), increasing the number of lines improves the reconstruction quality, and the RMSE decreases. Similarly, the relative uncertainty also decreases, indicating reduced sensitivity to measurement errors. On the right of the Fig. 4, it can be observed that, as the viewing angles increase, the reconstruction improves significantly, while the relative uncertainty, although lower than with two angles, appears to remain unchanged. This means that a given acquisition geometry can produce reconstructions of better quality but can also be more sensitive to measurement errors.

4. Indicators

As observed from the previous examples, given a detection geometry, the reconstruction quality can be assessed by comparing the reconstructed image with the phantom. Additionally, by examining the uncertainty propagation, the sensitivity to measurement errors can be understood. To evaluate a given geometry, two synthetic indicators are introduced to provide a concise overview of the geometry.

The first is called the geometric coverage in the following. It indicates the ability to reconstruct accurately the emission in a given region and is proportional to the number of lines passing through that region. In detail, it is defined for each pixel as the sum of all the geometric factors intersecting that pixel. The geometric coverage can be calculated as the product of the geometry projection matrix H and the vector $\boldsymbol{1}$ defined as a vector of ones with the same length as the number of projections, as reported in Eq. (11).

$$G = H * 1 \tag{11}$$

The second can be called the error factor. It indicates the uncertainty propagated by the system in each pixel, also determining the potential incidence of artifacts in any region of the cross-section. The error factor is evaluated as the uncertainty ε_i associated to each pixel when reconstructing a homogenous phantom of emissivity equal to 1.

Fig. 5 shows the geometric coverage and the error factor for the geometry reported on the right, which consists of 6 angles and a total of 120 lines.

From the geometric coverage, it can be observed that the areas with fewer intersections on the left side of the section are those where lower accuracy can be expected. From the error factor, it is possible to identify regions where greater error propagation or artifact production is likely.

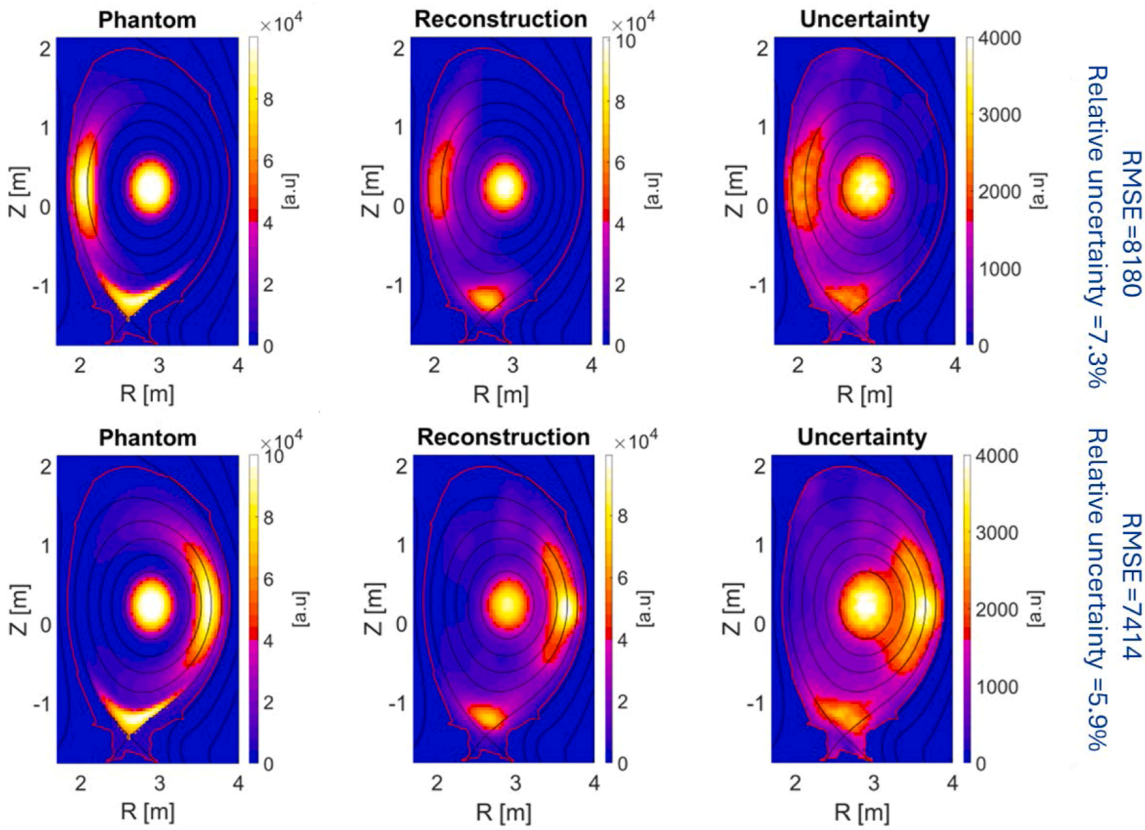

Fig. 6. Phantom (left), Reconstruction (Middle), Uncertainty (right). The magnetic field lines are reported to guide the eye but are not used in the reconstruction.

In this geometry, the top-left or centre-left areas of the cross-section are particularly vulnerable to showing artefacts.

In Fig. 6, the reconstructions and errors for two complex phantoms are shown, using the geometry of Fig. 5 (right). Although the reconstruction is not perfect, it is noticeable how the emission shapes are reconstructed without the need to introduce information from other diagnostics.

5. Conclusions and future developments

This work is aimed at presenting an innovative approach for the design of systems measuring line-integrals such as bolometers and SXR tomographies. The idea is to determine a geometric layout, in compliance with design constraints, that best optimizes reconstruction resolution and sensitivity to measurement errors. Using the maximum likelihood algorithm, it has been shown how different geometries can yield varying results. In particular, a given layout can provide more accurate reconstructions but be more sensitive to measurement errors and therefore associate larger uncertainties to the local emissivities. By introducing two original metrics, the geometric coverage and the error factor, it is possible to perform a comprehensive analysis of an acquisition geometry. Based on this method, the geometry can be optimized by properly weighting these indicators depending on the requirements and priorities of the design. The cases reported exemplify optimizations without the knowledge of the magnetic topology, corresponding to the aim of minimizing the dependence on prior information and of supporting real-time operation. Taking into account the geometry of the magnetic surfaces, to maximize the scientific exploitation in offline analysis, would be an immediate extension of the proposed methodology. It should be mentioned though that other design aspects, such as the dimensions of the viewing cones, the sensitivity to the deformations of the hardware in operating conditions and overlap of adjacent lines of sight, can have also a significant impact on the quality of the final reconstructions. These aspects are beyond the scope of the present paper but will be addressed in the very near future.

CRediT authorship contribution statement

Ivan Wyss: Writing – original draft, Software, Methodology, Formal analysis, Data curation, Conceptualization. **Valentina D'Agostino:** Writing – review & editing, Software. **Andrea Murari:** Writing – review & editing, Supervision, Methodology, Conceptualization. **Pasquale Gaudio:** Writing – review & editing, Supervision, Funding acquisition. **Michela Gelfusa:** Writing – review & editing, Funding acquisition. **Gerarda Apruzzese:** Supervision. **Riccardo Rossi:** Writing – review & editing, Supervision, Conceptualization.

Declaration of competing interest

The authors declare no conflict of interest.

Data availability

Data will be made available on request.

References

[1] P. David, M. Bernert, T. Pütterich, C. Fuchs, S. Glöggler, T. Eich, Optimization of the computation of total and local radiated power at ASDEX Upgrade, Nucl. Fusion 61 (6) (2021), https://doi.org/10.1088/1741-4326/abf2e1. Jun.
[2] G. Pucella, et al., Onset of tearing modes in plasma termination on JET: The role of temperature hollowing and edge cooling, Nucl. Fusion 61 (4) (2021), https://doi.org/10.1088/1741-4326/ABE3C7. Apr.
[3] I. Wyss et al., "Comparison of a fast low spatial resolution inversion method and peaking factors for the detection of anomalous radiation patterns and disruption prediction," 2023, doi: 10.1016/j.fusengdes.2023.113625.
[4] R. Rossi, et al., A systematic investigation of radiation collapse for disruption avoidance and prevention on JET tokamak, Matter Radiat. Extremes 8 (4) (2023), https://doi.org/10.1063/5.0143193. Jul.

[5] A. Murari, et al., Investigating the thermal stability of highly radiative discharges on JET with a new tomographic method, Nucl. Fusion 60 (4) (2020) 046030, https://doi.org/10.1088/1741-4326/AB7536. Mar.
[6] M. Bernert, et al., The X-Point radiating regime at ASDEX Upgrade and TCV, Nucl. Mater. Energy 34 (2023) 101376, https://doi.org/10.1016/J.NME.2023.101376. Mar.
[7] U. Stroth, et al., Model for access and stability of the X-point radiator and the threshold for marfes in tokamak plasmas, Nuclear Fusion 62 (7) (2022), https://doi.org/10.1088/1741-4326/ac613a. Jul.
[8] M. Groth, et al., Characterisation of divertor detachment onset in JET-ILW hydrogen, deuterium, tritium and deuterium-tritium low-confinement mode plasmas, Nuclear Mater. Energy 34 (2023), https://doi.org/10.1016/j.nme.2022.101345.
[9] H. Meister, et al., Bolometer developments in diagnostics for magnetic confinement fusion, J. Instrum. (2019), https://doi.org/10.1088/1748-0221/14/10/C10004. IOP Publishing LtdOct.
[10] K. Ertl, W. Von Der Linden, V. Dose, and A. Weller, "Maximum entropy based reconstruction of soft Xray emissivity profiles in W7-AS," 1996.
[11] M. Anton et al., "X-ray tomography on the TCV Tokamak," 1996.
[12] K. Moser, A. Bock, P. David, M. Bernert, R. Fischer, Gaussian process tomography at ASDEX upgrade with magnetic equilibrium information and nonstationary kernels, Fusion Sci. Technol. 78 (8) (2022) 607–616, https://doi.org/10.1080/15361055.2022.2072659.
[13] S. Xu, et al., An optimization method for ITER radial x-ray camera line-of-sight design basing on Bayesian uncertainty analysis, Plasma Phys. Control Fusion. 66 (6) (2024), https://doi.org/10.1088/1361-6587/ad3e2a. Jun.
[14] D. Pacella, et al., X-ray diagnostic developments in the perspective of DEMO, in: AIP Conf Proc 1612, . 2014, pp. 23–30, https://doi.org/10.1063/1.4894019. Aug.
[15] H. Meister, F. Penzel, Z. Szabo-Balint, R. Reichle, L.C. Ingesson, Performance estimations for the ITER bolometer diagnostic, Fusion Eng. Des. 146 (. 2019) 1015–1018, https://doi.org/10.1016/j.fusengdes.2019.01.146. Sep.
[16] T. Craciunescu, et al., Maximum likelihood bolometry for ASDEX upgrade experiments, Phys. Scr. 98 (12) (. 2023), https://doi.org/10.1088/1402-4896/ad081e. Dec.
[17] A. Huber, et al., Upgraded bolometer system on JET for improved radiation measurements, Fusion Eng. Des. 82 (5–14) (. 2007) 1327–1334, https://doi.org/10.1016/j.fusengdes.2007.03.027. Oct.
[18] L. C. Ingesson, C. F. Maggi, and R. Reichle, "Characterization of geometrical detection-system properties for two-dimensional tomography," 2000.
[19] M. Carr et al., "Description of complex viewing geometries of fusion tomography diagnostics by ray-tracing," Aug. 01, 2018, American Institute of Physics Inc. doi:10.1063/1.5031087.
[20] E. Peluso, et al., Dealing with artefacts in JET iterative bolometric tomography using masks, Plasma Phys. Control Fusion. 64 (4) (. 2022), https://doi.org/10.1088/1361-6587/ac4854. Apr.
[21] T. Craciunescu, E. Peluso, A. Murari, M. Gelfusa, Maximum likelihood bolometric tomography for the determination of the uncertainties in the radiation emission on JET TOKAMAK, Rev. Sci. Instrum. 89 (5) (2018), https://doi.org/10.1063/1.5027880. May.
[22] J. Qi, "A unified noise analysis for iterative image estimation," 2003.
[23] M. Odstrcil, J. Mlynar, T. Odstrcil, B. Alper, A. Murari, Modern numerical methods for plasma tomography optimisation, Nucl. Instrum. Methods Phys. Res. a 686 (. 2012) 156–161, https://doi.org/10.1016/j.nima.2012.05.063. Sep.
[24] J. Mlynar, et al., Current research into applications of tomography for fusion diagnostics, J. Fusion Energy 38 (3–4) (. 2019) 458–466, https://doi.org/10.1007/s10894-018-0178-x. Aug.